# A Cytosolic Bypass and G6P Shunt in Plants Lacking Peroxisomal Hydroxypyruvate Reductase[1[OPEN]]

**Jiying Li,[a,2] Sarathi M. Weraduwage,[a] Alyssa L. Preiser,[a] Stefanie Tietz,[a] Sean E. Weise,[a,b] Deserah D. Strand,[a,3] John E. Froehlich,[a,b] David M. Kramer,[a,b] Jianping Hu,[a,c] and Thomas D. Sharkey[a,b,d,4,5]**

[a]Michigan State University-Department of Energy Plant Research Laboratory, Michigan State University, East Lansing, Michigan 48824
[b]Department of Biochemistry and Molecular Biology, Michigan State University, East Lansing, Michigan 48824
[c]Department of Plant Biology, Michigan State University, East Lansing, Michigan 48824
[d]Plant Resilience Institute, Michigan State University, East Lansing, Michigan 48824

**ORCID IDs: 0000-0002-6180-3814 (J.L.); 0000-0002-0591-4210 (S.M.W.); 0000-0003-1293-1163 (S.T.); 0000-0002-4635-4299 (J.H.); 0000-0002-4423-3223 (T.D.S.).**

The oxygenation of ribulose 1,5-bisphosphate by Rubisco is the first step in photorespiration and reduces the efficiency of photosynthesis in $C_3$ plants. Our recent data indicate that mutants in photorespiration have increased rates of photosynthetic cyclic electron flow around photosystem I. We investigated mutant lines lacking peroxisomal hydroxypyruvate reductase to determine if there are connections between 2-phosphoglycolate accumulation and cyclic electron flow in Arabidopsis (*Arabidopsis thaliana*). We found that 2-phosphoglycolate is a competitive inhibitor of triose phosphate isomerase, an enzyme in the Calvin-Benson cycle that converts glyceraldehyde 3-phosphate to dihydroxyacetone phosphate. This block in metabolism could be overcome if glyceraldehyde 3-phosphate is exported to the cytosol, where cytosolic triose phosphate isomerase could convert it to dihydroxyacetone phosphate. We found evidence that carbon is reimported as glucose-6-phosphate, forming a cytosolic bypass around the block of stromal triose phosphate isomerase. However, this also stimulates a glucose-6-phosphate shunt, which consumes ATP, which can be compensated by higher rates of cyclic electron flow.

Photorespiration occurs when ribulose bisphosphate is oxygenated instead of carboxylated by Rubisco (Bowes et al., 1971). Oxygenation is an unavoidable consequence of the reaction mechanism of Rubisco, and once oxygenation occurs the remainder of photorespiratory metabolism reduces the cost of oxygenation (Andrews and Lorimer, 1978). Photorespiration reduces photosynthesis by three mechanisms: (1) reduction of Rubisco efficiency (increase in apparent $K_m$ for $CO_2$); (2) diversion of ATP and NADPH from carboxylation products to the photorespiratory pathway; and (3) release of $CO_2$ in the photorespiratory pathway. These three effects significantly reduce the photosynthetic rate in $C_3$ plants (Sharkey, 1988) and likely provided evolutionary pressure that resulted in $C_4$ metabolism (Sage et al., 2012). Photorespiration is also a source of hydrogen peroxide and can affect the redox status of plant cells (Foyer et al., 2009).

Although photorespiration will decline as atmospheric $CO_2$ increases, it will remain a significant issue for $C_3$ photosynthesis for a long time (Walker et al., 2016b). Using a spreadsheet available from a recent study (Sharkey, 2016), it can be calculated that the ratio of oxygenation to carboxylation at 25°C for a plant with Rubisco with the same kinetics found in Arabidopsis (*Arabidopsis thaliana*) would be 0.53 at the preindustrial $CO_2$ level of 290 $\mu$L $L^{-1}$, 0.39 at today's level of ~400 $\mu$L $L^{-1}$, and 0.26 when the $CO_2$ concentration is 600 $\mu$L $L^{-1}$ (assuming that $CO_2$ at Rubisco is 50% of that in air because of diffusion resistances at the stomata and in the mesophyll). Engineering alternative photorespiration pathways to ameliorate the negative effects of photorespiration on plant growth is currently under investigation (Kebeish et al., 2007; Peterhänsel et al., 2013;

[1]This work was supported by the U.S. Department of Energy (DE-FG02-91ER2002) and by partial salary support for T.D.S. from Michigan AgBioResearch.

[2]Present address: Microsoft Corporation, 1 Microsoft Way, Redmond, WA 98052.

[3]Present address: Max-Planck-Institut für Molekulare Pflanzenphysiologie, Am Mühlenberg 1, 14476 Potsdam-Golm, Germany.

[4]Author for contact: tsharkey@msu.edu.

[5]Senior author.

The author responsible for distribution of materials integral to the findings presented in this article in accordance with the policy described in the Instructions for Authors (www.plantphysiol.org) is: Thomas D. Sharkey (tsharkey@msu.edu).

J.L., D.M.K., and J.H. conceived the original screening and research plans; J.L., S.M.W., A.L.P., D.D.S., and J.E.F. performed most of the experiments; S.T. carried out the CEF measurements; S.E.W. provided technical assistance to J.L.; J.L., S.E.W., and T.D.S. designed the experiments and analyzed the data; T.D.S. wrote the article with contributions of all the authors.

[OPEN]Articles can be viewed without a subscription.
www.plantphysiol.org/cgi/doi/10.1104/pp.19.00256

  

Dalal et al., 2015; Xin et al., 2015; Betti et al., 2016; Engqvist and Maurino, 2017).

Photorespiratory metabolism converts two molecules of the first product of oxygenation, 2-phosphoglycolate (2-PG), to one molecule of 3-phosphoglycerate and one molecule of $CO_2$. Ordinarily, photorespiration proceeds at the rate needed to metabolize all of the 2-PG produced by oxygenation. Douce and Heldt (2000) conclude that "the only control step in the photorespiratory cycle is the level of competition between $O_2$ and $CO_2$ for binding to Rubisco." A number of the enzymes and transporters needed for photorespiration were discovered because plants lacking genes for these proteins can grow in a high-$CO_2$ atmosphere but not in air (Somerville and Ogren, 1979; Somerville, 1984).

It is assumed that the intermediates of photorespiration reduce the capacity of the Calvin-Benson cycle (Timm et al., 2016). Anderson (1971) showed that a very low concentration of 2-PG significantly inhibited triose phosphate isomerase (TPI), an enzyme that converts glyceraldehyde 3-phosphate (GAP) to dihydroxyacetone phosphate (DHAP). Somerville and Ogren (1979) showed that plants lacking phosphoglycolate phosphatase accumulate 2-PG and, based on Anderson's work, proposed that this would cause more triose phosphate to be exported from chloroplasts, favoring Suc synthesis. By altering the amount of phosphoglycolate phosphatase, Flügel et al. (2017) confirmed the inhibition of TPI by 2-PG and found less starch in plants with high 2-PG but did not find increased Suc. Xu et al. (2009) reported that plants lacking some glycolate oxidase activity had reduced activation of Rubisco and less mRNA for Rubisco activase than controls when grown in air but more Rubisco activase mRNA when grown in elevated $CO_2$ (0.5%). Walker et al. (2016a) found a reduced Rubisco activation ratio in plants lacking the plastidic glycerate/glycolate transporter (PLGG1). Flügge et al. (1980) showed that glyoxylate could cause acidification of the stroma and so inhibit pH-sensitive enzymes in the Calvin-Benson cycle, but this effect was not specific to glyoxylate, as other organic acids had the same effect. Kelly and Latzko (1976) reported that 2-PG (but not glycolate) inhibited phosphofructokinase, which they postulated could interfere with starch breakdown at night. However, there should be no 2-PG present when starch is breaking down, and current thinking about starch breakdown does not include a role for phosphofructokinase (Stitt and Zeeman, 2012). On the other hand, glycolate buildup has been suggested to protect PSII from oxidative stress (Messant et al., 2018). Finally, South et al. (2019) showed that engineered plants can accumulate glycolate and glyoxylate and still grow better than wild-type plants. Thus, 2-PG appears to be the toxic metabolite that must be detoxified by photorespiratory metabolism, and the effect of 2PG on TPI is the primary mechanism of toxicity.

Most of the enzymes and transporters of photorespiratory metabolism are essential; plants that lack them are very stunted or die when grown in air. However, plants missing NADH-dependent, peroxisomal hydroxypyruvate reductase in the peroxisome (*hpr1*) show only modest effects (Timm et al., 2008, 2012; Cousins et al., 2011). It is known that hydroxypyruvate can leave the peroxisome and be acted on by a cytosolic HPR (encoded by *HPR2*) that prefers NADPH (Kleczkowski et al., 1988; Timm et al., 2008). In addition, there is a multifunctional glyoxylate/hydroxypyruvate reductase in the chloroplast that prefers NADPH (Tolbert et al., 1970) that has now been identified as HPR3 (Timm et al., 2011). Loss of *HPR1* and *HPR2*, or all three, results in severe growth defects in air but not high $CO_2$ (Timm et al., 2008, 2011; Cousins et al., 2011). In addition, it has been hypothesized that some carbon leaves the photorespiratory pathway as Gly or Ser (Harley and Sharkey, 1991; Busch et al., 2018). Despite these alternatives, plants lacking *HPR1* are typically stunted, indicating that reduction of hydroxypyruvate is necessary for optimal photosynthesis.

In a recent survey of mutants of peroxisomal proteins using the Dynamic Environment Phenotype Imager (Cruz et al., 2016), many of the mutants exhibited significant phenotypes under high and fluctuating light but little phenotype under the low, constant light normally used to grow Arabidopsis. For instance, *hpr1-1*, *plgg1*, and *cat2-1* showed significant increases in cyclic electron flow around PSI (CEF; Li et al., 2019).

In this study, we investigated potential mechanisms by which plants respond to the loss of TPI activity resulting from 2-PG buildup. HPR1 was chosen as the focus of the study because *hpr1* plants grow reasonably well but still show a strong stimulation of CEF. Also, HPR1 was identified as playing a role in drought tolerance (Li and Hu, 2015).We measured amounts of accumulated 2-PG. We then looked at how 2-PG might affect the Calvin-Benson cycle and how those effects might lead to CEF. We postulate that the block of stromal TPI can be bypassed by export of GAP from chloroplasts to the cytosol followed by reimport of carbon into the chloroplast as Glc-6-P. However, this cytosolic bypass of the gluconeogenic reactions of the Calvin-Benson cycle leads to a stimulation of a Glc-6-P shunt (Sharkey and Weise, 2016; Sharkey, 2019) that consumes ATP, leading to CEF.

## RESULTS

### Growth, Chlorophyll and Carotenoid Contents, and Rubisco Activity of *hpr1* Plants

Both *hpr1-1* and *hpr1-2* plants showed a stunted phenotype when grown in air in these experiments (Fig. 1A). In addition to being smaller, the mutants had significantly less chlorophyll (Fig. 1B) and carotenoid (Fig. 1C) than the wild-type Columbia-0 (Col-0). On the other hand, the total extractable activity of Rubisco was the same in all three lines (Fig. 2A). The amount of Rubisco activase protein was less in the two mutant lines than in the

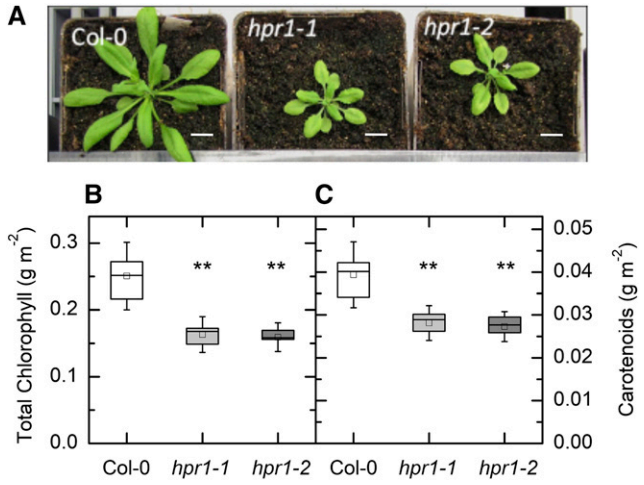


**Figure 1.** Rosette appearance of wild-type, *hpr1-1*, and *hpr1-2* plants and pigments. A, Photographs of three lines of Arabidopsis grown in soil for 4 weeks. Bars = 0.5 inches. B and C, Chlorophyll (B) and carotenoid (C) contents. Chlorophyll and carotenoids from the leaves of 4-week-old plants were measured as described in "Materials and Methods." Differences between the wild type and treatments were tested by one-way ANOVA followed by Tukey's test. The box encompasses the middle two quartiles, the mean is shown as an open square inside the box, the median is shown as a line inside the box, and the whiskers show the SD of the data. Statistical differences are indicated as follows: **, $\alpha = 0.01$. $n = 6$.

wild type (Fig. 2B). The activation state of Rubisco was modestly lower in low light (125 $\mu$mol $m^{-2}$ $s^{-1}$) in *hpr1-1* but not *hpr1-2* (Fig. 2C). After incubation in high light (1,000 $\mu$mol photons $m^{-2}$ $s^{-1}$), the activation state of Rubisco was higher in all three lines but did not differ among lines (Fig. 2D).

### 2-PG Content of Leaves Is High in *hpr1-1* and *hpr1-2*

The content of 2-PG was measured by liquid chromatography-tandem mass spectrometry (LC/MS-MS). The results are expressed as peak area for 2-PG relative to the peak area of the internal standard ([$^{13}C_6$] fructose [Fru]-1,6-bisP). The 2-PG content was significantly increased in the *hpr1-1* plants compared with the wild-type plants (Fig. 3). In *hpr1-2* plants, the level appeared higher than in wild-type plants (Fig. 3), but the difference did not reach statistical significance.

### Effect of 2-PG on TPI Activity

The effect of 2-PG on TPI was tested. 2-PG was a strong inhibitor of TPI and was competitive with GAP (Fig. 4). The inhibition constant, $K_i$, was 24.2 $\mu$M, between the two values reported previously (Anderson, 1971; Flügel et al., 2017). The relative effect this would have on TPI depends on the concentrations of GAP and 2-PG. To test whether the 2-PG was limiting the activity of TPI in vivo, we measured the concentrations of the triose phosphates. The concentration of DHAP was the same in Col-0 and *hpr1-1*, but the concentration of GAP was about 2-fold higher in *hpr1-1* than in Col-0 (note that GAP data have been multiplied by 10; Fig. 5). Because GAP is the first molecule produced in the stroma, an inhibition of TPI would be expected to cause a buildup of GAP. At equilibrium, the DHAP:GAP ratio is expected to be 21.5 (Sharkey and Weise, 2012). In Col-0, this ratio was 11.3, and in *hpr1-1*, the ratio was 6.1, consistent with a block in TPI activity affecting the Calvin-Benson cycle but also consistent with lack of equilibrium in Col-0.

### Expression of the *GPT2* Gene

It has been hypothesized that plants that lack chloroplastic Fru bisphosphatase might create a bypass by exporting more carbon to the cytosol and then reimporting carbon, possibly as Glc-6-P, through the glucose-6-phosphate/phosphate transporter 2 (GPT2; Kossmann et al., 1994; Sharkey and Weise, 2016). We tested whether the *hpr1-1* plants with inhibited stromal TPI could make use of cytosolic TPI (since there would be no 2-PG in the cytosol) by reimporting carbon as

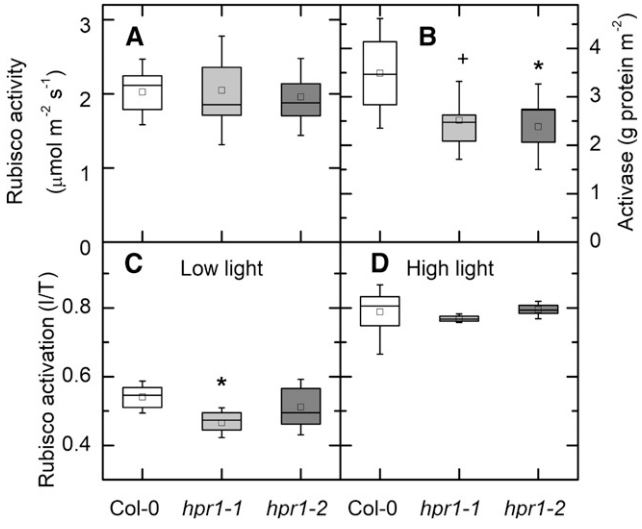


**Figure 2.** Rubisco activity and activase protein. A and B, Total Rubisco activity (A) and Rubisco activase protein (B). Activase protein was measured using antibodies raised against Rubisco activase and a WES capillary electrophoresis instrument from ProteinSimple. C and D, Rubisco activation state is presented as the ratio between initial (I; measured as quickly as possible after extraction) and total (T; after incubation with $HCO_3$ and Mg) at 125 (C) or 1,000 (D) $\mu$mol photons $m^{-2}$ $s^{-1}$. For A, C, and D, $n = 4$ to 7. For B, data were not different between the low-light and high-light treatments and so were combined ($n = 7$ or 8). Differences between the wild type and treatments were tested by one-way ANOVA followed by Tukey's test. The box encompasses the middle two quartiles, the mean is shown as an open square inside the box, the median is shown as a line inside the box, and the whiskers show the SD of the data. Statistical differences are indicated as follows: +, $\alpha = 0.1$ and *, $\alpha = 0.05$.

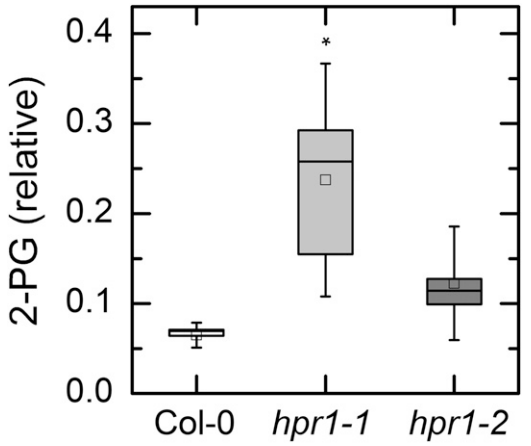


**Figure 3.** 2-PG content in leaves of Col-0 and two HPR mutants. 2-PG was measured by HPLC/MS-MS. Leaves were harvested after 6 h in 125 or 1,000 $\mu$mol photons $m^{-2}$ $s^{-1}$. Because the data for both light intensities were indistinguishable, they were combined to increase statistical power. Data are expressed as peak area of 2-PG divided by peak area of the internal standard relative to the weight of plant material extracted. The results in high and low light were not different and so all of the data were combined. Differences between the wild type and treatments were tested by one-way ANOVA followed by Tukey's test. The box encompasses the middle two quartiles, the mean is shown as an open square inside the box, the median is shown as a line inside the box, and the whiskers show the SD of the data. Statistical differences are indicated as follows: *, $\alpha = 0.05$. $n = 7$ or 8.

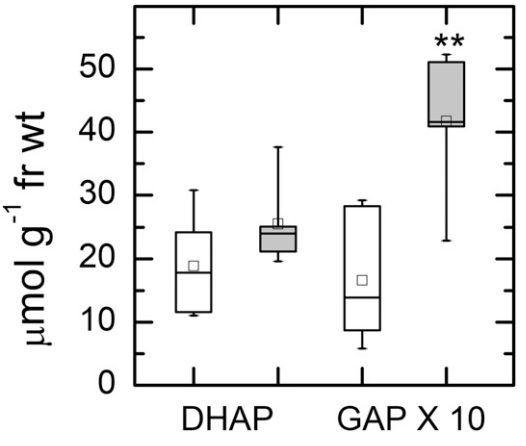


**Figure 5.** Amounts of DHAP and GAP. Leaves were treated with 1,000 $\mu$mol photons $m^{-2}$ $s^{-1}$ for 6 h and then clamped with liquid nitrogen-cooled copper blocks to stop metabolism in the light. Leaf samples were extracted with perchloric acid, neutralized, and then measured using sequential additions of GAP dehydrogenase and TPI while following NADH production photometrically. White boxes represent data for Col-0 and gray boxes represent data for *hpr1-1*. Differences between the wild type and treatments were tested by one-way ANOVA followed by Tukey's test. The box encompasses the middle two quartiles, the mean is shown as an open square inside the box, the median is shown as a line inside the box, and the whiskers show the SD of the data. Statistical difference is indicated as follows: **, $\alpha = 0.01$. $n = 5$. fr wt, Fresh weight.

Glc-6-P through the GPT2 transporter. When plants were grown and sampled in low light (125 $\mu$mol photons $m^{-2}$ $s^{-1}$), there was no difference in the transcript levels for *GPT2* (Fig. 6A). However, after exposing plants to 1,000 $\mu$mol photons $m^{-2}$ $s^{-1}$ for 6 h, transcripts for *GPT2* were up 4-fold in Col-0 plants and 10-fold in *hpr1-1* plants (note the 10-fold difference in the scale; Fig. 6B). Plants lacking the *plgg1* also had increased *GPT2* expression. These plants have increased glycolate (Pick et al., 2013) and presumably 2-PG, as found in the *hpr1-1* mutant.

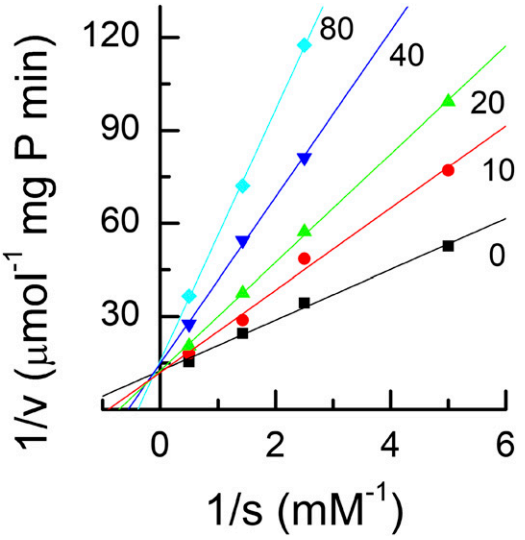


**Figure 4.** Lineweaver-Burk plot of TPI activity. TPI in crude extracts of Arabidopsis leaves was assayed in the presence of a range of GAP and 2-PG concentrations. The number on each line indicates the concentration of 2-PG in $\mu$M. The crossover of the lines at the *y* axis indicates that 2-PG is a competitive inhibitor.

### Unlabeled $CO_2$ Release and Cyclic Electron Flow

The import of Glc-6-P into the chloroplast could stimulate the oxidative branch of the pentose phosphate pathway, creating a Glc-6-P shunt (Sharkey and Weise, 2016). It is hypothesized that this should result in more $CO_2$ release during photosynthesis (day respiration or respiration in the light [$R_L$]) and a higher rate of cyclic electron flow. The $CO_2$ released during photosynthesis can be detected as a $^{12}CO_2$ flux from the leaf while the leaf is fed 99% $^{13}CO_2$. Both *hpr1* lines had higher $R_L$ for many minutes after switching from $^{12}CO_2$ to $^{13}CO_2$ (Fig. 7).

Increased cyclic electron flow has been reported for these lines (Li et al., 2019). We have repeated these measurements and found strong signals for cyclic electron flow. A plot of steady-state proton flux ($v_{H^+}$), measured as the initial slope of the decay of the electrochromic shift, versus linear electron flow measured by chlorophyll fluorescence (LEF) revealed more proton flux in the mutant plants than in wild-type plants at

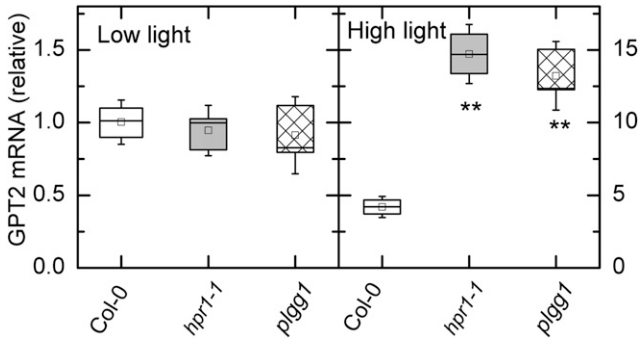


**Figure 6.** Reverse transcription quantitative PCR analysis of *GPT2* transcripts in low and high light. Transcripts were measured in two photorespiratory mutant lines and the wild type (Col-0) in plants taken from low light intensity (125 $\mu$mol $m^{-2}$ $s^{-1}$) and after 6 h (A) and high light (500 $\mu$mol $m^{-2}$ $s^{-1}$; B). Note that the scale is 10-fold higher for the high-light data, thus *GPT2* transcript was about 4-fold higher in Col-0 after the high-light treatment and about 15-fold higher in the *hpr1* mutants. Differences between the wild type and treatments were tested by one-way ANOVA followed by Tukey's test. The box encompasses the middle two quartiles, the mean is shown as an open square inside the box, the median is shown as a line inside the box, and the whiskers show the SD of the data. Statistical differences are indicated as follows: **, $\alpha = 0.01$. $n = 3$.

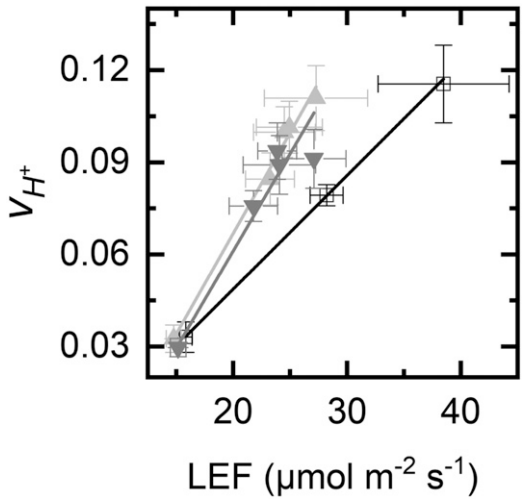


**Figure 8.** Cyclic electron flow in *hpr1* mutants. The plot shows $v_{H^+}$ versus LEF (measured by chlorophyll fluorescence quenching analysis). The error bars indicate SD. The linear regressions were $y = 0.0037x - 0.025$, $R^2 = 0.9997$ for Col-0 (white squares/black line), $y = 0.0053x - 0.0064$, $R^2 = 0.995$ for *hpr1-1* (upward triangles, light gray line), and $y = 0.0063x - 0.065$, $R^2 = 0.97$ for *hpr1-2* (downward triangles, dark gray line).

an equal LEF (Fig. 8). The slope of the linear regression was 0.0037 for Col-0 but averaged 0.0058 for the *hpr1* mutants.

## DISCUSSION

Inhibition of photorespiratory metabolism, except when this is achieved by reducing Rubisco oxygenase activity, results in reduced plant health. A major cause is reduced activity of TPI because of competitive inhibition by 2-PG. Glycolate and glyoxylate can accumulate without reducing plant health (South et al., 2019). Flügel et al. (2017) showed that 2-PG inhibition of TPI led to reduced Fru-1,6-bisP and also sedoheptulose 1,7-bisphosphate, two metabolites that require DHAP for synthesis. Although 2-PG is near the beginning of the pathway and HPR is near the end, loss of HPR activity caused a buildup of 2-PG. In this study, we found that the ratio of DHAP to GAP was reduced by nearly 50% in *hpr1-1* compared with Col-0, demonstrating that the measured inhibition of TPI by 2-PG affected metabolism in photosynthesizing leaves. The data in Figure 5 is for whole leaves, and it is likely that the disequilibrium is worse, possibly much worse, inside the chloroplast. The triose phosphates were not in equilibrium even in the wild-type Col-0. A lack of equilibrium at this step was hypothesized in the original report of the Calvin-Benson cycle (Bassham et al., 1954). They suggested that a lack of equilibrium in this step could explain their observed lower-than-predicted labeling of carbon 4 in sedoheptulose bisphosphate during very short labeling. The lack of equilibrium at TPI can also explain the Gibbs effect, in which hexose C4 is more heavily labeled than C3 (Kandler and Gibbs, 1956; Gibbs and Kandler, 1957). There are other factors that can lead to disequilibrium of label in carbons 3 and 4 (Ebenhöh and Spelberg, 2018), but the TPI disequilibrium significantly exacerbates the reduced labeling of carbon 3 relative to carbon 4.

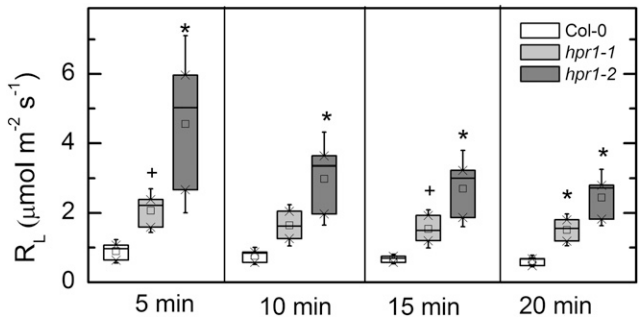


**Figure 7.** $R_L$ in Col-0 and *hpr1* mutants. $R_L$ was measured as the flux of $^{12}CO_2$ occurring when a leaf was fed 99% (mol/mol) $^{13}CO_2$. The LI-COR LI-800 gas analyzer is only 2.4% as sensitive for $^{13}CO_2$ as for $^{12}CO_2$, and it was assumed that the $^{13}CO_2$ concentration in the air stream was the same as the $^{12}CO_2$ had been before beginning the labeling. Differences between the wild type and treatments were tested by one-way ANOVA followed by Tukey's test. The box encompasses the middle two quartiles, the mean is shown as an open square inside the box, the median is shown as a line inside the box, and the whiskers show the SD of the data. Statistical differences are indicated as follows: +, $\alpha = 0.1$ and *, $\alpha = 0.05$. $n = 3$.

The disequilibrium at TPI can make the energetics of aldolase more favorable, as discussed by Sharkey (2019). It is therefore likely that the capacity for TPI is kept low

to keep the ratio of DHAP to GAP closer to 1 (optimal) than to 20 (equilibrium ratio). Therefore, despite its reputation for efficiency, TPI activity is not in excess during photosynthesis and the inhibition of TPI by 2-PG can have a significant effect on metabolism. To overcome the inhibition of TPI, GAP can be exported to the cytosol, where, in the absence of 2-PG, TPI can function.

We also tested whether Rubisco activase could play a role in the inhibition of photosynthesis when photorespiratory metabolism is blocked. The growth conditions used in our study resulted in smaller plants with less chlorophyll and carotenoids per leaf area (Fig. 1), and hence the block in photorespiration was affecting plant growth. However, the total activity of Rubisco was the same in Col-0 and two *hpr1* mutant lines (Fig. 2A). The amount of Rubisco activase protein was less in the mutant lines (Fig. 2B), consistent with the observation of reduced Rubisco activase message seen by Xu et al. (2009), but Rubisco activation state was lower in only one line and only at low light (Fig. 2C). Although this could affect how well plants cope with a stochastic light environment (Taylor and Long, 2017), we conclude from these results that effects on Rubisco activation may be secondary to the main effects of TPI inhibition, and the rest of this discussion will focus on the possible consequences of TPI inhibition.

Export of carbon for processing in the cytosol, as proposed here for TPI inhibition, has been proposed for other mutants. Sharkey and Weise (2016) hypothesized that a block in stromal fructose-1,6- bisphosphatatse (FBPase) can be bypassed by export of carbon to the cytosol. Carbon is then reimported into the chloroplast beyond the FBPase step in the Calvin-Benson cycle (Kossmann et al., 1994; Sharkey and Weise, 2016). A mutant lacking Fru-1,6-bisP aldolase also exhibits high rates of CEF (Gotoh et al., 2010). In this mutant, carbon could be exported as triose phosphates and then reimported as Glc-6-P to bypass the Fru-1,6-bisP aldolase step. We hypothesize that in these three cases (and perhaps others) carbon can be exported to the cytosol to bypass missing or limited enzymes of the Calvin-Benson cycle and then reimported into the chloroplast.

However, the gradient for triose phosphate reimport is unfavorable. The phosphate concentration is much higher in the cytosol than in the stroma (Sharkey and Vanderveer, 1989), which aids in triose phosphate export but would slow triose phosphate reimport. On the other hand, the gradient for Glc-6-P is highly favorable for import into the chloroplast (Gerhardt et al., 1987; Sharkey and Vassey, 1989; Szecowka et al., 2013) and could overcome the unfavorable phosphate gradient. Stimulation of *GPT2* expression would allow carbon to be reimported into the chloroplast as Glc-6-P. Transcripts for *GPT2* were elevated in *hpr1-1* and *plgg1* (Fig. 6). We saw that 2-PG was elevated in *hpr1-1*. Pick et al. (2013) saw that glycolate is elevated in *plgg1*, and it is very likely that 2-PG is also elevated in this mutant.

Figure 9 shows a model for the metabolic changes in *hpr1*. In Col-0, carbon is exported from the chloroplast for Suc synthesis, but once cytosolic FBPase acts, the carbon can no longer return to the chloroplast because there is only minimal capacity for Glc-1-P import (Fettke et al., 2011) and normally no capacity for Glc-6-P import, as evidenced by the large gradient in Glc-6-P between the cytosol and chloroplast (Weise et al., 2006). However, in the *hpr1* mutants, 2-PG accumulates and inhibits TPI. GAP can be exported and DHAP can be made in the cytosol because 2-PG is restricted to the chloroplast. However, phosphate is in high concentration in the cytosol and much lower in the chloroplast (Sharkey and Vanderveer, 1989), making it difficult for DHAP to be imported into the stroma at sufficiently high rates. Moreover, the high concentrations of triose phosphates in the cytosol could lead to Fru-1,6-bisP synthesis and dephosphorylation. Once Fru-1,6-bisP is converted to Fru-6-P by cytosolic FBPase, carbon could only reenter the stroma as hexose phosphate. Induction of GPT2 would allow carbon to be reimported as Glc-6-P. Once Glc-6-P is reimported into the chloroplast, it can rejoin the Calvin-Benson cycle if it is converted to Fru-6-P by phosphoglucoisomerase (PGI). This would result in a cytosolic bypass around the inhibited TPI.

However, stromal PGI is kinetically limited (Backhausen et al., 1997). The Fru-6-P:Glc-6-P ratio is normally 1:1 in the stroma, well below the predicted ratio and well below the ratio found in the cytosol (Gerhardt et al., 1987; Sharkey and Vassey, 1989; Szecowka et al., 2013). The $K_m$ of PGI for Glc-6-P is much higher than the $K_m$ for Fru-6-P (Schnarrenberger and Oeser, 1974; Table 1 of that article shows the opposite, but this is in error, as can be deduced from the text and abstract and as confirmed by our own unpublished results). In addition, the Calvin-Benson cycle would be limited by the lack of triose phosphates needed for transketolase and sedoheptulose bisphosphate synthesis.

Induction of GPT2 would result in a very high concentration of Glc-6-P in the stroma. Glc-6-P dehydrogenase has reduced activity during the day (Lendzian and Ziegler, 1970), but the effect is to increase the $K_m$ (Scheibe et al., 1989; Hauschild and von Schaewen, 2003). Therefore, a high concentration of Glc-6-P could overcome the light-induced changes in Glc-6-P dehydrogenase that normally restrict its activity during the day. This would stimulate the oxidative branch of the pentose phosphate pathway, making a Glc-6-P shunt around the Calvin-Benson cycle (Sharkey and Weise, 2016).

The Glc-6-P shunt results in a release of $CO_2$. This release would appear similar to the release of $CO_2$ during photorespiration. Cousins et al. (2011) reported that *hpr1-1* mutants exhibited higher than expected $CO_2$ release that was oxygen dependent. Plants lacking peroxisomal malate dehydrogenase, needed for HPR1 function, also released more than expected amounts of $CO_2$ (Cousins et al., 2008). We speculate that the excess $CO_2$ release seen in these studies results from the $CO_2$ released during the Glc-6-P shunt. Figure 7 shows that the extra $CO_2$ released is not rapidly labeled and persists for at least 20 min after switching isotopes. This is not consistent with a photorespiratory origin of this

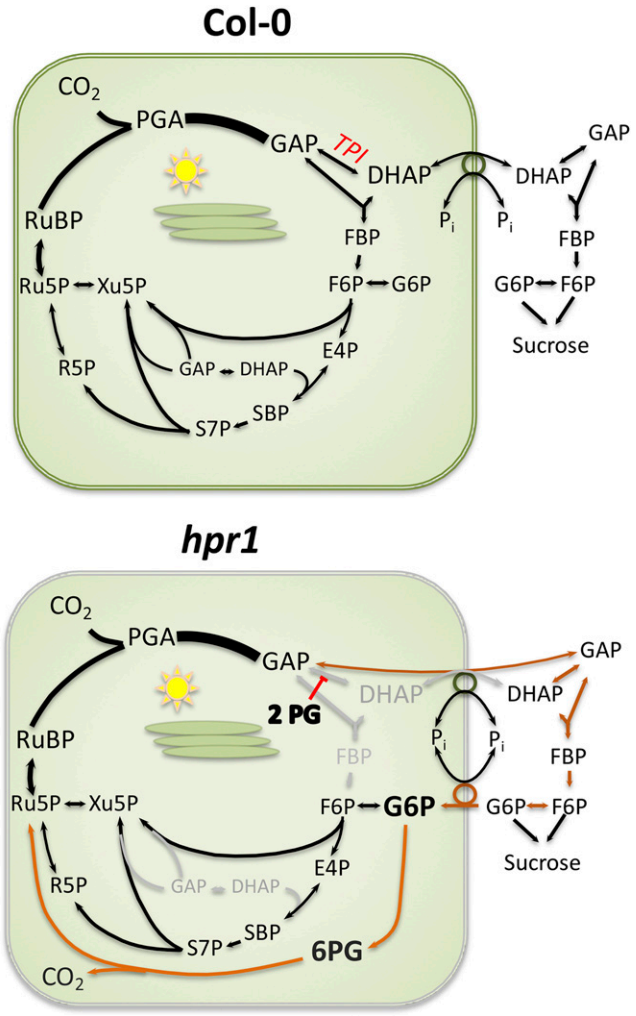


**Figure 9.** Hypothesized carbon flow in Col-0 and *hpr1-1*. The canonical path of carbon in the Calvin-Benson cycle plus Suc synthesis is shown for Col-0. In *hpr1-1* plants, we hypothesize that 2-PG inhibits TPI, forcing export of GAP. Once acted on by cytosolic TPI, some DHAP will be reimported, but the gradient in phosphate is not favorable for this flux. The triose phosphates in the cytosol will be converted eventually to Glc-6-P. Some unknown signal results in the expression of *GPT2*, allowing reimport of carbon as Glc-6-P. This allows some Calvin-Benson cycle activity but also stimulates the Glc-6-P shunt (shown in orange). Alternatively, Glc-6-P in the cytosol could build up and allow a cytosolic shunt in which ribulose 5-phosphate (Ru5P) is converted to xylulose 5-phosphate (Xu5P), which returns to the Calvin-Benson cycle through the xylulose phosphate transporter (not shown). The stimulated Glc-6-P shunt is balanced in terms of carbon and NADPH but reduces ATP availability. Another unknown signal results in cyclic electron flow. E4P, Erythrose 4-phosphate; F6P, Fru-6-P; PGA, phosphoglyceric acid; 6PG, 6-phosphoglucanate; R5P, ribose 5-phosphate; RuBP, ribulose 1,5-bisphosphate, SBP, sedoheptulose 1,7-bisphosphate; S7P, sedoheptulose 7-phosphate.

$CO_2$ release but is consistent with release of $CO_2$ by 6-phosphogluconate dehydrogenase in the Glc-6-P shunt if the shunt is involved in the slow-to-label carbon pool, as has been speculated (Sharkey, 2019).

The Glc-6-P shunt consumes three ATPs but is balanced for NADPH and carbon. Stimulation of this shunt would require significantly more ATP, and so CEF could be favored. We confirmed the observation, originally reported by Li et al. (2019); Fig. 8), that *hpr1* plants have increased cyclic electron flow. A buildup of hydrogen peroxide is a likely candidate for the signal that stimulates cyclic electron flow in these plants (Strand et al., 2017).

This provides a mechanism for connecting carbon metabolism changes with electron transport changes. If true, then other photorespiratory mutants that had been shown to contain elevated 2-PG levels should also show elevated CEF. Other mutants that reduce stromal Fru-1,6-bisP should also show elevated CEF because carbon would avoid these blockages through the cytosolic bypass, leading to increased rates of the Glc-6-P shunt. Gotoh et al. (2010) reported a strong stimulation of CEF in a mutant lacking stromal Fru-1,6-bisP aldolase, and plants lacking stromal FBPase also have high rates of cyclic electron flow (Livingston et al., 2010), which is consistent with a cytosolic bypass leading to a Glc-6-P shunt (Fig. 9).

Hydoxypyruvate reductase is only required if a significant amount of carbon that originates as 2-PG completes the photorespiratory pathway and becomes glycerate or $CO_2$. Some hydroxypyruvate can be reduced by other HPRs (Tolbert et al., 1970; Kleczkowski et al., 1988; Timm et al., 2008, 2011; Cousins et al., 2011). In addition, there are indications that some carbon can leave the photorespiratory cycle as Gly or Ser, but that would be limited by how fast nitrogen is made available (Harley and Sharkey, 1991; Busch et al., 2018). While the effect of the loss of HPR1 alone is not as great as the loss of other photorespiratory enzymes, for example 2-PG phosphatase (Somerville and Ogren, 1979), it nevertheless can impair plant growth, indicating that a significant fraction of carbon that begins the photorespiratory cycle as a result of oxygenation is reduced by HPR1 and completes the cycle. Nevertheless, because of the alternative paths for hydroxypyruvate reduction, *hpr1* plants are useful for study of the effects of an impairment, but not loss, of photorespiration.

We have reported new results, especially the disequilibrium of the triose phosphates and the high rate of apparent $R_L$. We have confirmed several other findings, such as the effect of 2-PG on TPI and the high rate of cyclic electron flow in *hpr1* plants. We have developed a comprehensive hypothesis that explains how 2-PG exerts its toxic effects and how both carbon metabolism and photosynthetic electron transport respond to this toxicity.

## MATERIALS AND METHODS

### Plant Material

Arabidopsis (*Arabidopsis thaliana*) Col-0, *hpr1-1*, and *hpr1-2* were used. The *hpr1* plants (SALK_067724 and SALK_143584) were the same as reported on by Timm et al. (2008), who showed that no HPR protein was detectable. Plants were grown in Redi-earth potting medium (Sungro Horticulture) under a 16-h

photoperiod. Growth chamber conditions were as follows: 120 $\mu$mol $m^{-2}$ $s^{-1}$ light intensity, daytime and nighttime temperatures of 22°C to 23°C and 20°C, and 60% relative humidity. For high-light treatment, plants were exposed to a light intensity of 1,000 $\mu$mol $m^{-2}$ $s^{-1}$ for 6 h unless otherwise noted.

## Measurement of Chlorophyll and Carotenoid

For chlorophyll measurement, two leaf discs were harvested from 4-week-old rosettes, and chlorophyll was extracted in 2 mL of 96% (v/v) ethanol using a protocol modified from Lichtenthaler and Wellburn (1983). The homogenate was maintained under dark conditions to prevent chlorophyll degradation. Absorbance of each tube at 470, 649, and 665 nm was measured with a spectrophotometer. The chlorophyll *a*, chlorophyll *b*, and carotenoid contents were calculated as follows: chlorophyll *a* ($\mu$g $mL^{-1}$) = $13.95A_{665} - 6.88A_{649}$; chlorophyll *b* = $24.96A_{649} - 7.32A_{665}$; carotenoids = $(1{,}000A_{470} - 2.05C_a - 114.8C_b)/245$ (Lichtenthaler and Wellburn, 1983). Pigment concentration was expressed in g $m^{-2}$ leaf tissue.

## Measurement of Rubisco Activity and Protein Levels of Rubisco Activase

Leaves from 4-week-old rosettes were harvested quickly into liquid $N_2$ and stored in a −80°C freezer. Rubisco activity was measured using a protocol modified from Sharkey et al. (1986, 2001. Leaf tissue was ground with the aid of a Retch mill (Retsch), and protein was extracted into 2 mL of extraction buffer [50 mM 4-2(2-hydroxyethyl)-1-piperazine propane sulfonic acid (EPPS), pH 8, 30 mM NaCl, 10 mM mannitol, 5 mM $MgCl_2$, 2 mM EDTA, 5 mM DTT, 0.5% (v/v) Triton X-100, 1% polyvinylpolypyrrolidone (PVPP), 0.5% casein, and 1% protease inhibitor cocktail (P9599; Sigma-Aldrich)]. To obtain initial activity, 20 $\mu$L of extract was added to 80 $\mu$L of assay buffer [50 mM 4-2(2-hydroxyethyl)-1-piperazine propane sulfonic acid, pH 8, 5 mM $MgCl_2$, 0.2 mM EDTA, 0.5 mM ribulose bisphosphate, and 15 mM $H^{14}CO_3^-$] in a 7-mL scintillation vial. After a 1-min incubation, 100 $\mu$L of 1 M formic acid was added to stop the reaction and release unreacted bicarbonate. The mixture was then dried, and the amount of radioactivity that was fixed was determined with the aid of a liquid scintillation analyzer (Tri-Carb2800TR; Perkin-Elmer). In order to determine total activity, 200 $\mu$L of the initial extract was added to 20 $\mu$L of activating solution (to give final concentrations of 20 mM $MgCl_2$, 15 mM $H^{14}CO_3^-$, and 61 $\mu$M 6-phosphogluconate) and incubated for 10 min. Total Rubisco activity of the activated sample was assayed as explained above. Each day, radioactivity in 10 $\mu$L of the assay buffer was counted to determine specific activity. Based on 1 mCi = $2.22 \times 10^9$ distintegrations $min^{-1}$, initial and total Rubisco activity was calculated and expressed as $\mu$mol $m^{-2}$ $s^{-1}$. The rates were divided by 0.943 to account for the discrimination against $^{14}C$ (Roeske and O'Leary, 1984).

To determine Rubisco activase protein content, total protein was extracted from 4-week-old rosette leaves using a PlantTotal Protein Extraction Kit (PE0230; Sigma-Aldrich). Total protein concentration in the extracts was measured by carrying out a modified Lowry assay, and denaturing PAGE was performed to determine the purity and quality of the extracted protein. For quantification, equal amounts of total protein from each sample were loaded onto an automated capillary-based size western-blotting system (ProteinSimple; WES System). Rubisco activase in each protein sample was detected using antibodies raised against Rubisco activase (rabbit; AS10700; Agrisera). Data analysis was carried out using Compass Software (ProteinSimple).

## Measurement of 2-PG

Eight-week-old plants were treated with 125 or 1,000 $\mu$mol $m^{-2}$ $s^{-1}$ light for 6 h. After treatment, leaf tissue was harvested and immediately frozen in liquid nitrogen before being stored at −80°C. Samples were finely ground using a chilled mortar and pestle. Metabolites were extracted with 3:71:26 ethanol:formic acid:water (v/v/v). After centrifuging, the supernatant was freeze dried, resuspended in acetonitrile, and filtered through Mini-Uniprep Syringless Filter Devices (0.2 $\mu$m; GE Healthcare).

LC/MS-MS was carried out on an Acquity UPLC Performance LC (Waters) and Quattro Premier XE (Micromass) in electrospray negative ion mode. The column used was an Acquity UPLC BEH Amide (1.7 $\mu$m, 2.1 × 100 mm; Waters). Mass Lynx (v. 4.1; Waters) was used for data acquisition and analysis. Acquity Binary Solvent Manager (v. 1.40.1248) and Acquity Sample Manager (v. 1.40.2532) were used as the binary solvent manager. Capillary voltage was 2.75 kV, source temperature was 120°C, and desolvation temperature was 350°C. Desolvation gas flow was set to 800 L $h^{-1}$, and collision gas flow was 0.15 mL $min^{-1}$. Selected reaction monitoring was used to quantify levels of 2-PG. The parameters for monitoring 2-PG were trace of 153 > 97 (mass-to-charge ratio), cone voltage of 19 V, and collision energy of 17 V. Parameters for the internal standard ([$^{13}C_6$]Fru-1,6-bisP; Omicron) were trace of 345 > 97 (mass-to-charge ratio), cone voltage of 16 V, and collision energy of 25 V. A multistep gradient was used with 10 mM ammonium acetate in water (A) and acetonitrile (B). The flow rate was set to 0.3 mL $min^{-1}$ throughout the entire run: 0 to 1 min, 5% A; 1 to 1.5 min, 5% to 100% A; 1.5 to 3 min, 100% A; 3 to 3.5 min, 100% to 5% A; 3.5 to 4 min, 5% A (all % in v/v).

## Measurement of GAP, DHAP, and TPI

About 500 mg fresh weight of leaves was immediately freeze clamped using aluminum blocks cooled on dry ice to stop metabolism fast enough to measure triose phosphates. Samples were weighed and then fully pulverized using a Retsch Mill M300 (Retsch). Cold 3.5% (v/v) perchloric acid (2 $\mu$L $mg^{-1}$ tissue) was added, and tubes were placed on ice for 5 min of incubation. Extracts were centrifuged at maximum speed at 4°C for 10 min. Approximately 500 $\mu$L of supernatant was recovered. Neutralizing buffer (2 M KOH, 150 mM HEPES, and 10 mM KCl), in the ratio of 0.25 $\mu$L $\mu L^{-1}$ recovered supernatant, was added to the supernatant to bring the pH to ~7. pH sticks were used to check the pH; the volume of neutralizing buffer was adjusted accordingly, and the volume of neutralizing buffer was recorded. Samples were frozen and thawed to precipitate salts and then centrifuged at maximum speed for 2 min. The supernatant was pipetted off for immediate GAP and DHAP assays or frozen at −80°C for future assays.

The amount of GAP and DHAP was measured using a dual-wavelength filter photometer (ZFP22; Sigma-Aldrich). Supernatant (50 $\mu$L) was added to 800 $\mu$L of reaction buffer (100 mM HEPES buffer, pH 7.6, 1 mM DTT, 1 mM $KH_2AsO_4$, 50 mM NAD, and 50 mM ADP) in a cuvette, which was inserted into the cuvette holder in the spectrophotometer. Glyceraldehyde 3-phosphate dehydrogenase (5 units; G-5537; Sigma-Aldrich) was added to the cuvette and immediately mixed using a clean plastic stick. The difference of absorbance between the baseline and the maximum level was measured to estimate the level of GAP. Next, 5 units of TPI (T-6285; Sigma-Aldrich) was added to convert DHAP to GAP. We used $A_{334} - A_{405}$ and an extinction coefficient of 6,190 $M^{-1}$ $cm^{-1}$.

TPI activity was measured by linking the production of DHAP from GAP to oxidation of NADH to NAD through glycerophosphate dehydrogenase as described by Anderson (1971). TPI from crude protein extracts of Arabidopsis leaves harvested from 4-week-old rosettes was assayed in the presence of varying concentrations of GAP (0, 0.2, 0.4, 0.7, and 2 mM) and 2-PG (0, 10, 20, 40, and 80 $\mu$M). The same dual-wavelength filter photometer mentioned above was used to record the rate of change in absorbance at 334 − 405 nm.

## Reverse Transcription Quantitative PCR

Arabidopsis total RNA was isolated using a Plant RNeasy kit according to the manufacturer's instructions (Qiagen) and treated with DNase I. A total of 500 ng of each RNA sample was used for complementary DNA synthesis with random primers and the iScript complementary DNA Synthesis Kit (Bio-Rad). Reverse transcription quantitative PCR was performed using a 7500 Fast Real-Time PCR System with Fast SYBR Green Master Mix (Applied Biosystems). Gene expression was normalized to actin. Expression was determined in triplicate biological measurements.

## Determination of $R_L$

Plants were grown hydroponically on Rockwool under 8 h of light at 120 $\mu$mol $m^{-2}$ $s^{-1}$, 23°C, and 16 h of dark at 20°C. Plants were analyzed at 8 weeks. Plants were put in a LI-COR 6800 for 15 min to acclimate. The light intensity was set to 120 $\mu$mol $m^{-2}$ $s^{-1}$, dew point was approximately 18°C, and reference $CO_2$ was approximately 400 $\mu$L $L^{-1}$ (v/v). The flow rate was set to 400 $\mu$mol $s^{-1}$. After 15 min, 400 $\mu$L $L^{-1}$ $^{12}CO_2$ was rapidly switched to 400 $\mu$L $L^{-1}$ $^{13}CO_2$ ($^{99}$mol %). The gas was completely exchanged within 1.5 min. The output of the LI-COR 6800 was partitioned to a GasHound (LI-COR LI-800). This is the same instrument used by Loreto et al. (2001). This analyzer has a very low sensitivity to $^{13}CO_2$ (1.7% according to Loreto et al. [2001], 2.4% in our study). The LI-800 signal was corrected for the $^{13}CO_2$ as described by Loreto et al. (2001) so that the rate of release of $^{12}CO_2$ was measured. Photographs of the

photosynthetic surface area of each plant were taken, and area was calculated using Photoshop.

## Determination of Cyclic Electron Flow

Cyclic electron flow was determined by plotting $v_{H^+}$ as a function of linear electron flow as described previously (Li et al., 2019).

## Statistics and Box Plots

Differences between the wild type and treatments were tested by one-way ANOVA followed by Tukey's test in Microcal Origin 8.0. Three levels of significance were tested and indicated as follows: $^+$, $\alpha = 0.1$; *, $\alpha = 0.05$; and **, $\alpha = 0.01$. Box plots are presented with the box encompassing the middle two quartiles, the mean shown as an open square inside the box, the median shown as a line inside the box, and the whiskers showing the SD of the data.

## Accession Numbers

Accession numbers for the mutants used in this study are as follows: *hpr1-1*, SALK_067724; *hpr1-2*, SALK_ 143584; and *plgg1-1*, SALK_053469.

## ACKNOWLEDGMENTS

We thank Francesco Loreto and Susanna Pollastri for the loan of the $^{13}CO_2$-insensitive LI-800 $CO_2$ analyzer. We also thank Jim Klug and Cody Keilen for their assistance in growing plants, the Arabidopsis Biological Resource Center for seeds, and Andreas Weber for *plgg1* seeds. Antje von Schaewen made helpful comments on Figure 9.

Received March 6, 2019; accepted March 11, 2019; published March 18, 2019.

## LITERATURE CITED

**Anderson LE** (1971) Chloroplast and cytoplasmic enzymes. II. Pea leaf triose phosphate isomerases. Biochim Biophys Acta **235:** 237–244

**Andrews TJ, Lorimer GH** (1978) Photorespiration: Still unavoidable? FEBS Lett **90:** 1–9

**Backhausen JE, Jöstingmeyer P, Scheibe R** (1997) Competitive inhibition of spinach leaf phosphoglucose isomerase isoenzymes by erythrose 4-phosphate. Plant Sci **130:** 121–131

**Bassham JA, Benson AA, Kay LD, Harris AZ, Wilson AT, Calvin M** (1954) The path of carbon in photosynthesis. XXI. The cyclic regeneration of carbon dioxide acceptor. J Am Chem Soc **76:** 1760–1770

**Betti M, Bauwe H, Busch FA, Fernie AR, Keech O, Levey M, Ort DR, Parry MAJ, Sage R, Timm S, et al** (2016) Manipulating photorespiration to increase plant productivity: Recent advances and perspectives for crop improvement. J Exp Bot **67:** 2977–2988

**Bowes G, Ogren WL, Hageman RH** (1971) Phosphoglycolate production catalyzed by ribulose diphosphate carboxylase. Biochem Biophys Res Commun **45:** 716–722

**Busch FA, Sage RF, Farquhar GD** (2018) Plants increase $CO_2$ uptake by assimilating nitrogen via the photorespiratory pathway. Nat Plants **4:** 46–54

**Cousins AB, Pracharoenwattana I, Zhou W, Smith SM, Badger MR** (2008) Peroxisomal malate dehydrogenase is not essential for photorespiration in Arabidopsis but its absence causes an increase in the stoichiometry of photorespiratory $CO_2$ release. Plant Physiol **148:** 786–795

**Cousins AB, Walker BJ, Pracharoenwattana I, Smith SM, Badger MR** (2011) Peroxisomal hydroxypyruvate reductase is not essential for photorespiration in Arabidopsis but its absence causes an increase in the stoichiometry of photorespiratory $CO_2$ release. Photosynth Res **108:** 91–100

**Cruz JA, Savage LJ, Zegarac R, Hall CC, Satoh-Cruz M, Davis GA, Kovac WK, Chen J, Kramer DM** (2016) Dynamic environmental photosynthetic imaging reveals emergent phenotypes. Cell Syst **2:** 365–377

**Dalal J, Lopez H, Vasani NB, Hu Z, Swift JE, Yalamanchili R, Dvora M, Lin X, Xie D, Qu R, et al** (2015) A photorespiratory bypass increases plant growth and seed yield in biofuel crop *Camelina sativa*. Biotechnol Biofuels **8:** 175

**Douce R, Heldt HW** (2000) Photorespiration. *In* RC Leegood, S von Caemmerer, T Sharkey, eds, Photosynthesis: Physiology and Mechanisms. Kluwer, Dordrecht, The Netherlands, pp 115–136

**Ebenhöh O, Spelberg S** (2018) The importance of the photosynthetic Gibbs effect in the elucidation of the Calvin-Benson-Bassham cycle. Biochem Soc Trans **46:** 131–140

**Engqvist MKM, Maurino VG** (2017) Metabolic engineering of photorespiration. *In* AR Fernie, H Bauwe, APM Weber, eds, Photorespiration: Methods and Protocols. Springer, New York, pp 137–155

**Fettke J, Malinova I, Albrecht T, Hejazi M, Steup M** (2011) Glucose-1-phosphate transport into protoplasts and chloroplasts from leaves of Arabidopsis. Plant Physiol **155:** 1723–1734

**Flügel F, Timm S, Arrivault S, Florian A, Stitt M, Fernie AR, Bauwe H** (2017) The photorespiratory metabolite 2-phosphoglycolate regulates photosynthesis and starch accumulation in Arabidopsis. Plant Cell **29:** 2537–2551

**Flügge UI, Freisl M, Heldt HW** (1980) The mechanism of the control of carbon fixation by the pH in the chloroplast stroma: Studies with acid mediated proton transfer across the envelope. Planta **149:** 48–51

**Foyer CH, Bloom AJ, Queval G, Noctor G** (2009) Photorespiratory metabolism: Genes, mutants, energetics, and redox signaling. Annu Rev Plant Biol **60:** 455–484

**Gerhardt R, Stitt M, Heldt HW** (1987) Subcellular metabolite levels in spinach leaves: Regulation of sucrose synthesis during diurnal alterations in photosynthetic partitioning. Plant Physiol **83:** 399–407

**Gibbs M, Kandler O** (1957) Asymmetric distribution of $C^{14}$ in sugars formed during photosynthesis. Proc Natl Acad Sci USA **43:** 446–451

**Gotoh E, Matsumoto M, Ogawa K, Kobayashi Y, Tsuyama M** (2010) A qualitative analysis of the regulation of cyclic electron flow around photosystem I from the post-illumination chlorophyll fluorescence transient in Arabidopsis: A new platform for the in vivo investigation of the chloroplast redox state. Photosynth Res **103:** 111–123

**Harley PC, Sharkey TD** (1991) An improved model of $C_3$ photosynthesis at high $CO_2$: Reversed $O_2$ sensitivity explained by lack of glycerate reentry into the chloroplast. Photosynth Res **27:** 169–178

**Hauschild R, von Schaewen A** (2003) Differential regulation of glucose-6-phosphate dehydrogenase isoenzyme activities in potato. Plant Physiol **133:** 47–62

**Kandler O, Gibbs M** (1956) Asymmetric distribution of $C^{14}$ in the glucose phosphates formed during photosynthesis. Plant Physiol **31:** 411–412

**Kebeish R, Niessen M, Thiruveedhi K, Bari R, Hirsch HJ, Rosenkranz R, Stäbler N, Schönfeld B, Kreuzaler F, Peterhänsel C** (2007) Chloroplastic photorespiratory bypass increases photosynthesis and biomass production in *Arabidopsis thaliana*. Nat Biotechnol **25:** 593–599

**Kelly GJ, Latzko E** (1976) Inhibition of spinach-leaf phosphofructokinase by 2-phosphoglycollate. FEBS Lett **68:** 55–58

**Kleczkowski LA, Givan CV, Hodgson JM, Randall DD** (1988) Subcellular location of NADPH-dependent hydroxypyruvate reductase activity in leaf protoplasts of *Pisum sativum* L. and its role in photorespiratory metabolism. Plant Physiol **88:** 1182–1185

**Kossmann J, Sonnewald U, Willmitzer L** (1994) Reduction of the chloroplastic fructose-1,6-bisphosphatase in transgenic potato plants impairs photosynthesis and plant growth. Plant J **6:** 637–650

**Lendzian K, Ziegler H** (1970) Über die Regulation der Glucose-6-phosphat-Dehydrogenase in Spinatchloroplasten durch Licht. Planta **94:** 27–36

**Li J, Hu J** (2015) Using co-expression analysis and stress-based screens to uncover Arabidopsis peroxisomal proteins involved in drought response. PLoS ONE **10:** e0137762

**Li J, Tietz S, Cruz JA, Strand DD, Xu Y, Chen J, Kramer DM, Hu J** (2019) Photometric screens identified Arabidopsis peroxisome proteins that impact photosynthesis under dynamic light conditions. Plant J **97:** 460–474

**Lichtenthaler HK, Wellburn AR** (1983) Determination of total carotenoids and chlorophyll a and b of leaf extracts in different solvents. Biochem Soc Trans **603:** 591–592

**Livingston AK, Cruz JA, Kohzuma K, Dhingra A, Kramer DM** (2010) An Arabidopsis mutant with high cyclic electron flow around photosystem I (hcef) involving the NADPH dehydrogenase complex. Plant Cell **22:** 221–233

**Loreto F, Velikova V, Di Marco G** (2001) Respiration in the light measured by $^{12}CO_2$ emission in $^{13}CO_2$ atmosphere in maize leaves. Aust J Plant Physiol **28:** 1103–1108

**Messant M, Timm S, Fantuzzi A, Weckwerth W, Bauwe H, Rutherford AW, Krieger-Liszkay A** (2018) Glycolate induces redox tuning of photosystem II in vivo: Study of a photorespiration mutant. Plant Physiol **177:** 1277–1285

**Peterhänsel C, Krause K, Braun HP, Espie GS, Fernie AR, Hanson DT, Keech O, Maurino VG, Mielewczik M, Sage RF** (2013) Engineering photorespiration: Current state and future possibilities. Plant Biol (Stuttg) **15:** 754–758

**Pick TR, Bräutigam A, Schulz MA, Obata T, Fernie AR, Weber APM** (2013) PLGG1, a plastidic glycolate glycerate transporter, is required for photorespiration and defines a unique class of metabolite transporters. Proc Natl Acad Sci USA **110:** 3185–3190

**Roeske CA, O'Leary MH** (1984) Carbon isotope effects on enzyme-catalyzed carboxylation of ribulose bisphosphate. Biochemistry **23:** 6275–6284

**Sage RF, Sage TL, Kocacinar F** (2012) Photorespiration and the evolution of C4 photosynthesis. Annu Rev Plant Biol **63:** 19–47

**Scheibe R, Geissler A, Fickenscher K** (1989) Chloroplast glucose-6-phosphate dehydrogenase: $K_m$ shift upon light modulation and reduction. Arch Biochem Biophys **274:** 290–297

**Schnarrenberger C, Oeser A** (1974) Two isoenzymes of glucosephosphate isomerase from spinach leaves and their intracellular compartmentation. Eur J Biochem **45:** 77–82

**Sharkey TD** (1988) Estimating the rate of photorespiration in leaves. Physiol Plant **73:** 147–152

**Sharkey TD** (2016) What gas exchange data can tell us about photosynthesis. Plant Cell Environ **39:** 1161–1163

**Sharkey TD** (2019) Discovery of the canonical Calvin–Benson cycle. Photosynthesis Research10.1007/s11120-018-0600-2

**Sharkey TD, Vanderveer PJ** (1989) Stromal phosphate concentration is low during feedback limited photosynthesis. Plant Physiol **91:** 679–684

**Sharkey TD, Vassey TL** (1989) Low oxygen inhibition of photosynthesis is caused by inhibition of starch synthesis. Plant Physiol **90:** 385–387

**Sharkey TD, Weise SE** (2012) Autotrophic carbon dioxide fixation. *In* JJ Eaton-Rye, B Tripathy, TD Sharkey, eds, Photosynthesis: Plastid Biology, Energy Conversion and Carbon Assimilation. Springer Academic Publications, Dordrecht, The Netherlands, pp 649–672

**Sharkey TD, Weise SE** (2016) The glucose 6-phosphate shunt around the Calvin-Benson cycle. J Exp Bot **67:** 4067–4077

**Sharkey TD, Seemann JR, Berry JA** (1986) Regulation of ribulose-1,5-bisphosphate carboxylase activity in response to changing partial pressure of $O_2$ and light in *Phaseolus vulgaris*. Plant Physiol **81:** 788–791

**Sharkey TD, Badger MR, von Caemmerer S, Andrews TJ** (2001) Increased heat sensitivity of photosynthesis in tobacco plants with reduced Rubisco activase. Photosynth Res **67:** 147–156

**Somerville CR** (1984) The analysis of photosynthetic carbon dioxide fixation and photorespiration by mutant selection. Oxf Surv Plant Mol Cell Biol **1:** 103–131

**Somerville CR, Ogren WL** (1979) Phosphoglycolate phosphatase-deficient mutant of Arabidopsis. Nature **280:** 833–836

**South PF, Cavanagh AP, Liu HW, Ort DR** (2019) Synthetic glycolate metabolism pathways stimulate crop growth and productivity in the field. Science**363:** eaat9077

**Stitt M, Zeeman SC** (2012) Starch turnover: Pathways, regulation and role in growth. Curr Opin Plant Biol **15:** 282–292

**Strand DD, Livingston AK, Satoh-Cruz M, Koepke T, Enlow HM, Fisher N, Froehlich JE, Cruz JA, Minhas D, Hixson KK, et al** (2017) Defects in the expression of chloroplast proteins leads to $H_2O_2$ accumulation and activation of cyclic electron flow around photosystem I. Front Plant Sci **7:** 2073

**Szecowka M, Heise R, Tohge T, Nunes-Nesi A, Vosloh D, Huege J, Feil R, Lunn J, Nikoloski Z, Stitt M, et al** (2013) Metabolic fluxes in an illuminated *Arabidopsis* rosette. Plant Cell **25:** 694–714

**Taylor SH, Long SP** (2017) Slow induction of photosynthesis on shade to sun transitions in wheat may cost at least 21% of productivity. Philos Trans R Soc Lond B Biol Sci **372:** 20160543

**Timm S, Nunes-Nesi A, Pärnik T, Morgenthal K, Wienkoop S, Keerberg O, Weckwerth W, Kleczkowski LA, Fernie AR, Bauwe H** (2008) A cytosolic pathway for the conversion of hydroxypyruvate to glycerate during photorespiration in *Arabidopsis*. Plant Cell **20:** 2848–2859

**Timm S, Florian A, Jahnke K, Nunes-Nesi A, Fernie AR, Bauwe H** (2011) The hydroxypyruvate-reducing system in Arabidopsis: Multiple enzymes for the same end. Plant Physiol **155:** 694–705

**Timm S, Mielewczik M, Florian A, Frankenbach S, Dreissen A, Hocken N, Fernie AR, Walter A, Bauwe H** (2012) High-to-low $CO_2$ acclimation reveals plasticity of the photorespiratory pathway and indicates regulatory links to cellular metabolism of Arabidopsis. PLoS ONE **7:** e42809

**Timm S, Florian A, Fernie AR, Bauwe H** (2016) The regulatory interplay between photorespiration and photosynthesis. J Exp Bot **67:** 2923–2929

**Tolbert NE, Yamazaki RK, Oeser A** (1970) Localization and properties of hydroxypyruvate and glyoxylate reductases in spinach leaf particles. J Biol Chem **245:** 5129–5136

**Walker BJ, Skabelund DC, Busch FA, Ort DR** (2016a) An improved approach for measuring the impact of multiple $CO_2$ conductances on the apparent photorespiratory $CO_2$ compensation point through slope-intercept regression. Plant Cell Environ **39:** 1198–1203

**Walker BJ, VanLoocke A, Bernacchi CJ, Ort DR** (2016b) The costs of photorespiration to food production now and in the future. Annu Rev Plant Biol **67:** 107–129

**Weise SE, Schrader SM, Kleinbeck KR, Sharkey TD** (2006) Carbon balance and circadian regulation of hydrolytic and phosphorolytic breakdown of transitory starch. Plant Physiol **141:** 879–886

**Xin CP, Tholen D, Devloo V, Zhu XG** (2015) The benefits of photorespiratory bypasses: How can they work? Plant Physiol **167:** 574–585

**Xu H, Zhang J, Zeng J, Jiang L, Liu E, Peng C, He Z, Peng X** (2009) Inducible antisense suppression of glycolate oxidase reveals its strong regulation over photosynthesis in rice. J Exp Bot **60:** 1799–1809